Electronic Supplementary Information

Facile Tailoring the Two-Dimensional Graphene Oxide Channels for Gas Separation

*Jie Shen, Mengchen Zhang, Gongping Liu, Wanqin Jin**

State Key Laboratory of Materials-Oriented Chemical Engineering, Nanjing Tech University, 5 Xinmofan Road, Nanjing 210009, P.R. China. Correspondence and requests for materials should be addressed to W. Jin. (wqjin@njtech.edu.cn)

1. Experimental section

1.1 Materials

Graphite powder was provided by Nanjing XFNANO Co., Ltd. $NaNO_3$, H_2SO_4 (98 wt%), $KMnO_4$, H_2O_2 (30 wt%) and HCl (36.5 wt%) were purchased from Sinopharm Chemical Reagent Co., Ltd. PEBAX MH 1657 was provided from Arkema, France. Ethanol was supplied by Wuxi City Yasheng Chemical Co. Ltd. H_2, CO_2, N_2 and CH_4 gases with the purity of 99.999% were purchased from Nanjing Special Gases Company. Polyvinylidene fluoride (PVDF) supports with average pore size of 450 nm were obtained from Solvay, America. Deionized water was used in all the experiments.

1.2 Preparation and thermal annealing of GO

Graphene oxide (GO) was prepared by modified Hummer's method [1]. Typically, 10 g graphite powder and 5 g $NaNO_3$ were added into 230 mL 98 wt% H_2SO_4 under stirring for 1 h. Then 60 g $KMnO_4$ was slowly put into the mixture solution, and keep the temperature below 20 ℃ for about 2 h. The amount of $KMnO_4$ was larger than that in literature [1] because it can synthesize GO with higher oxidation degree. Subsequently, the reaction temperature was carefully increased to 35 ℃ and stirred for 0.5 h. Then, 460 mL deionized water was slowly

added into the system. After that, the mixture was heated to 98 ℃ and stirred for 15 min. The reaction was stopped by adding 1.4 L deionized water and followed by the addition of 100 mL H_2O_2 until the mixture turned yellow. The mixture was washed with 2 L 1mol/L HCl and a large amount of deionized water. The resulting solid was dried and dissolved in deionized water followed by sonication under 35 kHz for 0.5 h. The stable GO dispersion was finally obtained after centrifugation at 2000 rpm for 30 min. GO with different oxidation degrees were obtained by thermal annealing process. GO powders were heated under 180 ℃ for 5, 10 and 24 h in vacuum drying oven, respectively. Compared with the original GO, the reduced GO (rGO) lost a lot of oxygen-containing groups, which caused the decrease of O/C ratio. GO reduced under 180 ℃ for 5, 10 and 24 h were denoted as rGO-5 h, rGO-10 h and rGO-24 h, respectively.

1.3 Membrane preparation

Membranes were fabricated by solution casting method. GO, rGO-5h, rGO-10h and rGO-24h were dispersed in a solvent mixture of 70 wt% ethanol and 30 wt% water and then treated by ultrasonication for 1 h. Optimized by previous work [2], the mass content of GO was 0.1 wt% on the basis of the amount of PEBA polymer, namely (mGO/mPEBA) ×100 wt%=0.1 wt%, where mGO and mPEBA represent the weights of GO and PEBA polymer, respectively. After that, PEBA pellets were added into the solvent with stirring under 80 ℃ for 12 h. After eliminating the bubbles, the mixed solution was cast on PVDF substrate to fabricate flat composite membranes, which were used for gas permeation tests. The corresponding free-standing membranes were fabricated by casting the mixed solution onto the glass, which were used for other characterization. The membranes were finally formed by evaporating the solvent at room temperature for 2 days, then dried in a vacuum oven at 70 ℃ for 48 h. Also, the pure PEBA membrane was fabricated according to the similar procedure without the incorporation of GO.

1.4 Characterization

The dispersion and the sizes of GO nanosheets as well as the surface morphologies of as-prepared membranes were obtained by atomic force microscopy (AFM, XE-100, Park SYSTEMS, Korea) operated in the Non-contact mode. Fourier transform infrared (FTIR, AVATAR-FT-IR-360, Thermo Nicolet, USA) spectra was used to characterized the functionalized groups on GO. The thermal properties of GO and as-prepared membranes were characterized by thermogravimetric analysis (TGA, NETZSCH STA 449F3) in the range of room temperature to 800 or 1000 ℃ with the rate of 10 ℃ min^{-1}. The crystalline structure of GO with different O/C ratios were analyzed by X-ray diffraction (XRD, Bruker, D8 Advance) using Cu Kα radiation (λ=1.54 Å) at 40 kV and 15 mA at room temperature. Raman spectroscopy (LabRAM HR, HORIBA, France) was carried out with 514 nm wavelength incident laser light with the range of 500-4000 cm^{-1} to distinguish the ordered and disordered carbon structures. In order to study the effect of GO oxygenated groups on the chemical properties of as-prepared membranes, X-ray photoelectron spectroscopy (XPS, Thermo ESCALAB 250, USA) were carried out and recorded using monochromatized Al Ka radiation (1486.6 eV). Field emission scanning electron microscope (FESEM, S4800, Hitachi, Japan) was further used to observe the surface and cross-section of pure PEBA and GO-PEBA membranes. The CO_2 and N_2 adsorption behaviors of the as-prepared membranes were obtained by adsorption experiments at 25 ℃ (ASAP 2020, Micromeritics, USA).

1.5 Gas permeation measurements

Pure gas permeation was measured to investigate the gas transport behavior through the membranes using the constant-pressure, variable-volume method which was reported in our previous work [3]. The tests were conducted with a transmembrane pressure of 0.3 MPa at the temperature of 25 ℃. Gas flow rates were detected with a bubble flow meter in the following order: N_2, CH_4, H_2 and CO_2. The specimen was mounted onto the home-made permeation cell and the effective surface areas of flat composite membrane was 12.6 cm^2.

The mass transport in dense polymeric membranes follows the well-known solution-diffusion mechanism. The permeation measurements of each gas were performed at least 5 times with differences among them smaller than 2%. Gas permeability was calculated after the system reached steady-state using the following equation:

$$P = \frac{1}{\Delta p} \cdot \frac{273.15}{273.15+T} \cdot \frac{p_{atm}}{76} \cdot \frac{l}{A} \cdot \left(\frac{dV}{dt}\right) \quad (1)$$

where P is the gas permeability [1 Barrer = 10^{-10} cm^3 (STP) cm/ ($cm^2 \cdot s \cdot cmHg$)], Δp is the transmembrane pressure (atm), p_{atm} is the atmospheric pressure (atm), T is the temperature (℃), A is the membrane effective area (cm^2), and dV/dt is the volumetric displacement rate in the bubble flow meter.

The ideal separation factor which is the ratio of the permeability of the individual gas, can be expressed as follows:

$$\alpha = \frac{P_A}{P_B} \quad (2)$$

where P_A and P_B are the permeability of pure gas A and B, respectively.

2. Supplementary Figures and Tables

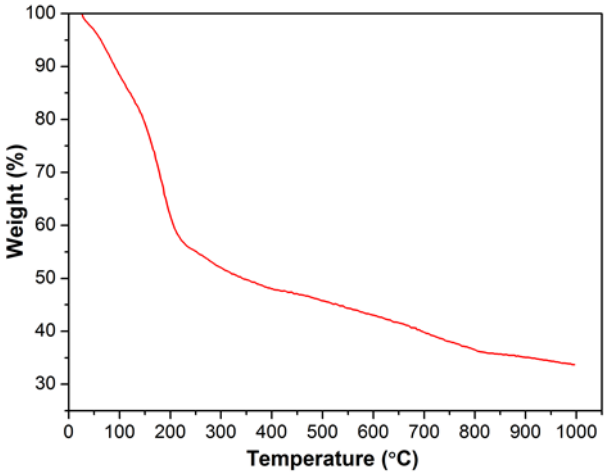

Fig. S1. TGA characterization for GO powder.

Thermogravimetric analysis (TGA) was carried out to study the thermal property of GO, which is displayed in Fig. S1. From room temperature to 100 ℃, the mass loss of GO powder is due to the removal of adsorbed water. When the temperature continued to increase, especially exceeded 150 ℃, the GO powder showed a sharp decrease which can be ascribed to the pyrolysis of the oxygen-containing functional groups on the GO sheets [4]. So we reduced GO under 180 ℃ for different length of time to obtain GO with distinct oxidation degrees.

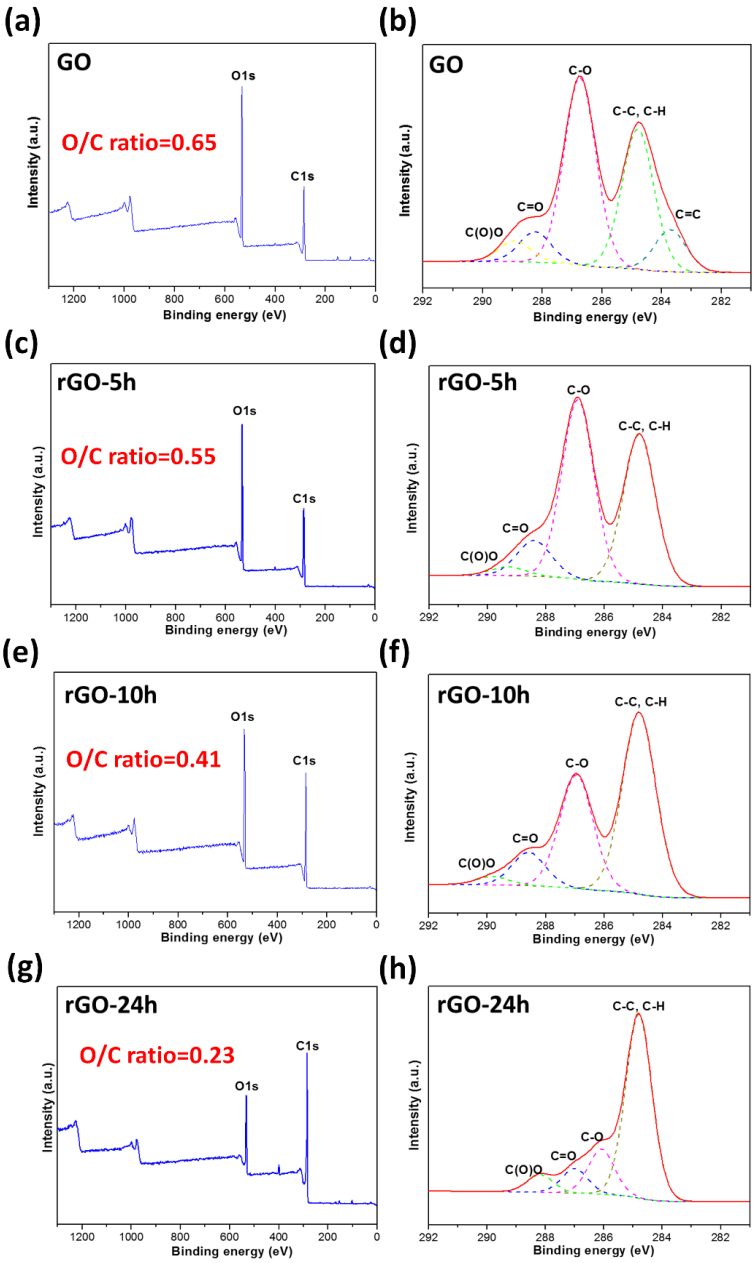

Fig. S2. XPS for GO and reduced GO. (a), (c), (e) and (g) are wide scan while (b), (d), (f) and (h) are the narrow scan for C1s.

Table S1. XPS data of GO

	Atomic content (%)
C=C	7.8
C-C	33.2
C-O	45.8
C=O	7.2
C(O)O	6.0
O/C ratio	0.65

Table S2. XPS data of rGO-5 h

	Atomic content (%)
C-C	39.6
C-O	47.5
C=O	10.3
C(O)O	2.6
O/C ratio	0.55

Table S3. XPS data of rGO-10 h

	Atomic content (%)
C-C	53.9
C-O	33.7
C=O	9.9
C(O)O	2.5
O/C ratio	0.41

Table S4. XPS data of rGO-24h

	Atomic content (%)
C-C	67.75
C-O	16.65
C=O	9.06
C(O)O	6.53
O/C ratio	0.23

The chemical properties of GO and reduced GO were further characterized by X-ray photoelectron spectroscopy (XPS) as shown in Fig. S2. The C1s spectrum of GO indicates four kinds of C atoms in different functional groups which are C=C (~283.7 eV), C-C, C-H (~284.5 eV), C-O (~286.8 eV), C=O (~288.4 eV), C(O)O (~289.7 eV). For pristine GO, the C-O groups takes up 45.8 % of the total C1s peak area while the content of C=O and C(O)O are 7.2 % and 6.0 %, respectively. This demonstrates that epoxy and hydroxyl groups occupy the majority of these functionalized groups on GO. The results show that the O/C ratio of GO is approximately 0.65, which is relatively high compared with the reported values [5]. However, the oxygen containing groups were gradually lost during the thermal annealing process which led to the decrease of O/C ratio. After heating at 180 ℃ for 24 h, the O/C ratio of rGO decreased to 0.23. All the XPS results were summarized in Tables S1-4 which are in agreement with FTIR characterization and prove the change of chemistry properties during the thermal reduction process.

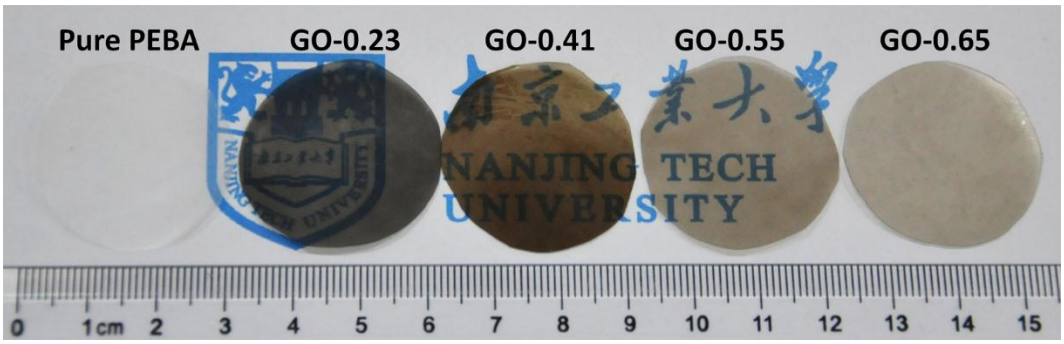

Fig. S3. Digital images of as-prepared free-standing membranes containing GO with different O/C ratios.

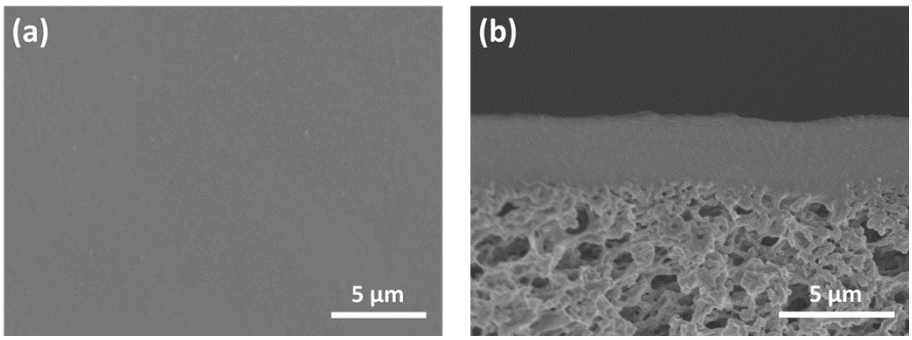

Fig. S4. SEM images of pure PEBA membrane (a) surface and (b) cross-section.

The surface of pure PEBA membrane is smooth without bulges and wrinkles. Cross-section images also showed flat PEBA membrane layer.

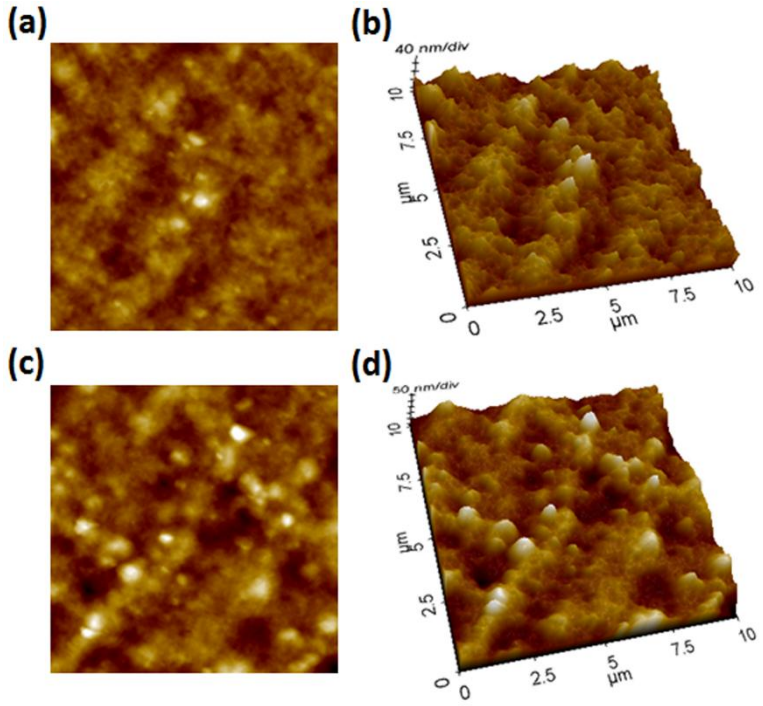

Fig. S5. AFM characterization for the membranes surfaces. (a) and (b) are pure PEBA membrane while (c) and (d) are GO-0.55 membrane. The scan area is 10 μm × 10 μm, 2D and 3D AFM images are presented left and right. See the surface roughness parameters in Table S5.

Table S5. Surface roughness parameters of membranes

Membrane	Pure PEBA	GO-0.55
Rq (nm)	19.585	30.002
Ra (nm)	15.119	23.168

As shown in Fig. S5 and Table S5, GO-0.55 membrane showed much higher surface roughness than that of pure PEBA membrane, which proves the presence of GO laminates in the membrane.

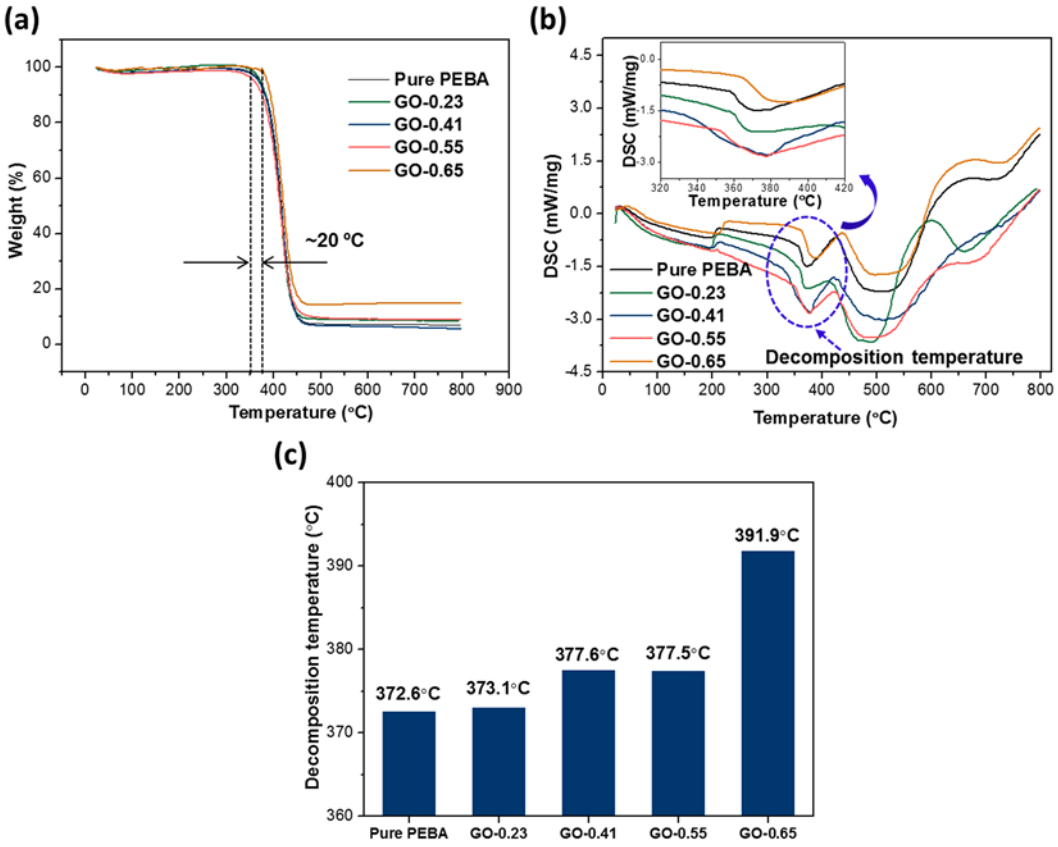

Fig. S6. (a) TGA and (b) DSC curves of membranes containing GO with different O/C ratios. Inserted in (b) shows the enlarged section with temperature ranging from 320 to 420 ℃. (c) Comparison of decomposition temperatures of different membranes.

Thermogravimetric analysis also indicates that GO-PEBA interactions were strengthened by increasing the GO O/C ratio. Fig. S6a shows that GO-0.65 membrane showed obviously enhanced decomposition temperature, which can be further proved by enlarged DSC curves (Fig. S6b). It could be found that the thermal stability of PEBA membrane can be improved by GO O/C ratio (Fig. S6c) because of the strong GO-polymer interactions (such as hydrogen bonding frameworks) can be formed between GO and PEBA polymer chains. In addition, membranes with low GO O/C ratio showed no obvious enhancement of decomposition temperature, which can also be ascribed to the poor dispersion of GO in polymeric environment.

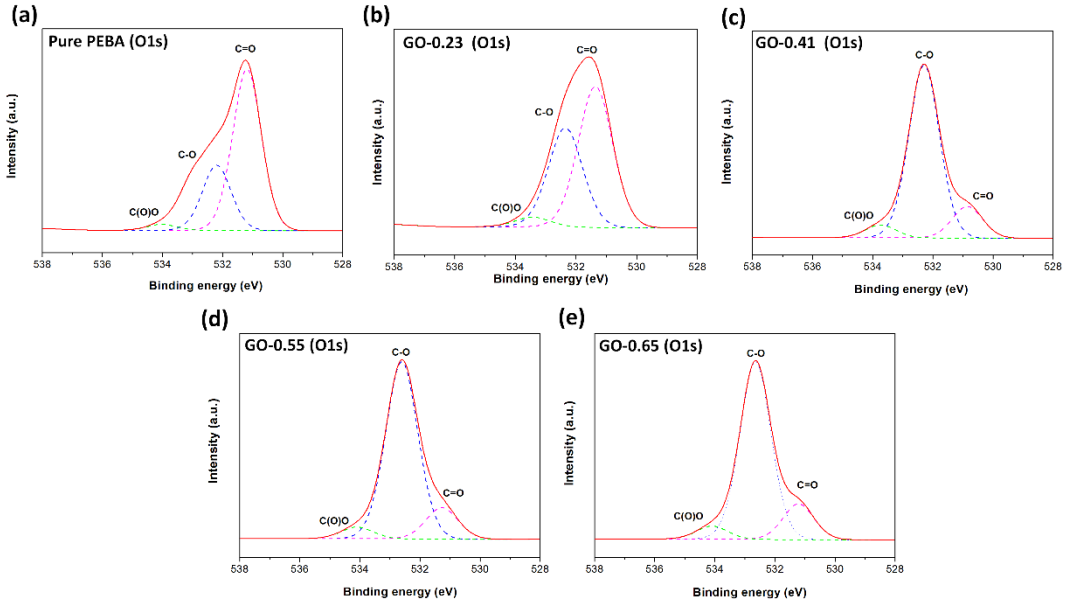

Fig. S7. XPS O1s spectra of pure PEBA, GO-0.23, GO-0.41, GO-0.55 and GO-0.65 membranes. See the data in Table S7.

Table S6. XPS O1s data of pure PEBA, GO-0.23, GO-0.41, GO-0.55 and GO-0.65 membranes

O1s Peak	Pure PEBA (eV)	GO-0.23 (eV)	GO-0.41 (eV)	GO-0.55 (eV)	GO-0.65 (eV)
C=O	531.09	531.21	530.92	531.27	531.42
C-O	532.19	532.20	532.25	532.41	532.65
C(O)O	533.99	533.78	533.94	534.10	534.19

The hydrogen bonding interactions between GO and PEBA chains were investigated by XPS O1s spectra. In Fig. S7 and Table S6, for GO-0.65 membrane, all of the O1s peaks shifted to higher binding energy (compared with those of pure PEBA membrane), indicating that O atoms could form hydrogen bonds with H atoms [6, 7]. However, after thermal reduction (GO-0.23 and GO-0.41 membranes), GO lost large number of oxygen-containing groups, which

weakened the hydrogen bonds between GO nanosheets and PEBA chains. Thus, the O1s characteristic peaks shifted to lower binding energy, as displayed in Fig. S7 and Table S6.

The enhanced hydrogen bonding frameworks with GO O/C ratio can also be proven by the gas permeation tests (Fig. 4 in main text). It should be noted that GO-0.65 membrane exhibited 20 % enhanced of CO_2 adsorption capability and 1.4 times larger interlayer empty space than that of GO-0.55 membrane, however, the CO_2 permeability increased only 6 % (from 97 Barrer of GO-0.55 to 103 Barrer of GO-0.65). That is because GO with more oxygen-containing groups caused strong GO-polymer interaction, which led to restriction of polymer chains mobility.

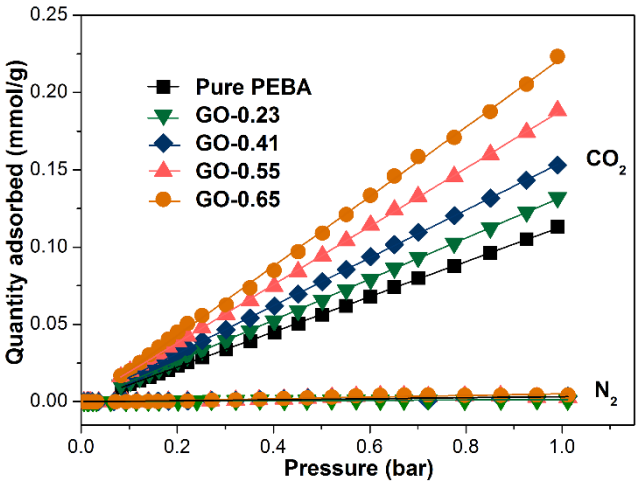

Fig. S8. Pure-component CO_2 and N_2 adsorptions (temperature: 25 ℃, pressure: 0-1 atm) on membranes containing GO with different GO O/C ratios, both of which follow single-site Langmuir models, K_D is Henry's constant. See the data in Table S8.

Table S7. Comparison of adsorption behaviors of membranes containing GO with different GO O/C ratios

Membrane	$K_{D,CO2}$ (mmol/g·bar)	$K_{D,N2}$ (mmol/g·bar)	Adsorption selectivity (CO_2/N_2)
Pure PEBA	0.114	0.005	22.8
GO-0.23	0.132	0.006	22.0
GO-0.41	0.155	0.006	25.8
GO-0.55	0.188	0.006	31.3
GO-0.65	0.225	0.006	37.5

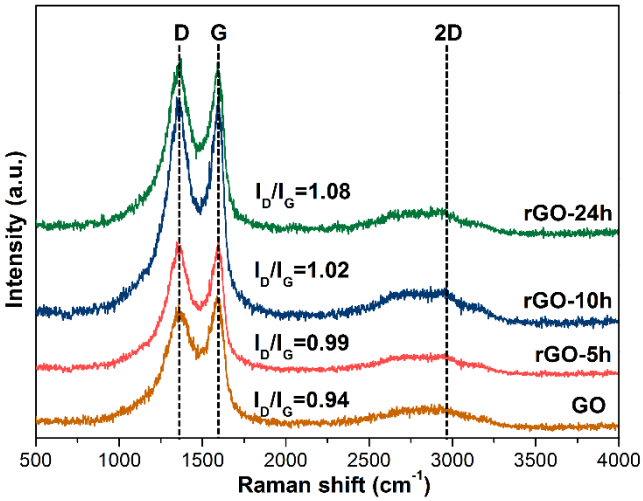

Fig. S9. Raman spectra of GO, rGO-5 h, rGO-5 h and rGO-24 h.

Raman spectroscopy was conducted to further analyze the structural changes during the thermal reduction process [8]. As shown in Fig. S10, both GO and rGO exhibit characteristic peaks of carbon materials which are D, G and 2D bands at approximately 1356, 1586 and 2870 cm^{-1}, respectively. D band is ascribed to defects or disorders on the graphene platelets and the G band refers to graphitized structure [9]. The value of I_D/I_G intensity ratio can be utilized to characterize the degree of local microdefects on graphene platelets. For pristine GO, the I_D/I_G is about 0.94 which is in consistent with the reported work [10]. However, the values of I_D/I_G were enlarged after the thermal reduction. The gradually increased I_D/I_G intensity ratio can be attributed to the microdefects generated by the loss of oxygen-containing groups during the thermal reduction which leads to the disorder [11].

3. Supplementary notes

3.1 Discussion on the gas transport mechanisms of membranes containing GO with different O/C ratios.

As shown in Fig. 1 in main text, when GO with high O/C ratio (0.65), the assembled laminates showed good dispersibility in polymeric environment. Although GO exhibited highest CO_2 adsorption ability, the interlayer spacing was too large, which allowed other larger molecules such as N_2 and CH_4 to transport through. So the gas permeability was the highest with the sacrifice of gas selectivity.

Moderate oxidized GO laminates (with O/C ratio of 0.55) also showed good dispersibility in polymer environment. More importantly, the interlayer empty space was manipulated to 0.36 nm, which allowed fast CO_2 permeation while blocked larger gases such as N_2 and CH_4. As a result, this membrane showed high CO_2 permeability and selectivity at the same time.

However, when GO was with a low content of oxygen-containing groups, the dispersibility was sharply weakened, which led to the gas barrier effect. The gas permeability was therefore decreased. What's worse, the interlayer empty space was too small to allow gas molecules to transport and CO_2 adsorption ability was significantly reduced, which is negative for CO_2 separation.

Supplementary References:

1 W. S. Hummers and R. E. Offeman, *J. Am. Chem. Soc.*, **1958**, *80*, 1339-1339.

2 J. Shen, G. Liu, K. Huang, W. Jin, K.-R. Lee, N. Xu, Angew. Chem. Int. Ed. **2015**, *54*, 578-582.

3 K. Huang, Z. Dong, Q. Li and W. Jin, *Chem. Commun.*, **2013**, *49*, 10326-10328.

4 J. I. Paredes, S. Villar-Rodil, A. Mart ínez-Alonso and J. M. D. Tasc ón, *Langmuir*, **2008**, *24*, 10560-10564.

5 S. Pei and H.-M. Cheng, *Carbon*, **2012**, *50*, 3210-3228.

6 N. I. Kovtyukhova, T. E. Mallouk, L. Pan and E. C. Dickey, *J. Am. Chem. Soc.*, **2003**, *125*, 9761-9769.

7 M. Yoonessi, Y. Shi, D. A. Scheiman, M. Lebron-Colon, D. M. Tigelaar, R. A. Weiss and M. A. Meador, *ACS Nano*, **2012**, *6*, 7644-7655.

8 A. C. Ferrari and D. M. Basko, *Nat. Nanotechol.*, **2013**, *8*, 235-246.

9 A. C. Ferrari, J. C. Meyer, V. Scardaci, C. Casiraghi, M. Lazzeri, F. Mauri, S. Piscanec, D. Jiang, K. S. Novoselov, S. Roth and A. K. Geim, *Phys. Rev. Lett.*, **2006**, *97*, 187401.

10 H. Li, Z. Song, X. Zhang, Y. Huang, S. Li, Y. Mao, H. J. Ploehn, Y. Bao and M. Yu, *Science*, **2013**, *342*, 95-98.

11 S. Stankovich, D. A. Dikin, R. D. Piner, K. A. Kohlhaas, A. Kleinhammes, Y. Jia, Y. Wu, S. T. Nguyen and R. S. Ruoff, *Carbon*, **2007**, *45*, 1558-1565.